# Nuclear structure of $^{126}$Xe

J. B. Gupta[1] and J. H. Hamilton [2,*]

[1]*Physics Department, Ramjas College, University of Delhi, Delhi-110 007, India*
[2]*Physics Department, Vanderbilt University, Nashville, Tennessee 37235, USA*

**Background:** The ($N < 82$)Xe isotopes with only four valence protons are known to be $\gamma$ soft and to have the spectrum similar to the O(6) limiting symmetry.

**Purpose:** Study the validity of the O(6) $\supset$ O(5) symmetry in the various vibrational bands of the $N = 72$ $^{126}$Xe isotope.

**Methods:** Comparison of the $^{126}$Xe spectrum with O(6) symmetry. Apply the microscopic theory of dynamic pairing plus quadrupole (DPPQ) model and the interacting boson model (IBM-1). The energy spectrum, absolute $B$(E2) values and E2 transition ratios are evaluated. The odd-even spin staggering in the $\gamma$ band is displayed, and the potential-energy plot is used to determine the shape of the nucleus.

**Results:** The predictions of the eigenvalues and the $B$(E2) values and the interband $B$(E2) ratios extended over the five excited bands up to $\tau = 5$ in the O(6) multiplet view. The O(5) symmetry is well preserved, and the O(6) symmetry is slightly broken.

**Conclusions:** The predictions in the DPPQ model provide an alternative framework to the fluctuations in the O(6) quantum numbers in the IBM framework. The DPPQ model predictions are in fair agreement with experiment. The IBM-1 predictions provide a complementary view.

## I. INTRODUCTION

The three dynamical symmetries U(5), SU(3), and O(6) of the algebraic group U(6) in the *sd*-interacting boson model (IBM-1) [1], provide analytical solutions of the collective Hamiltonian of the atomic nuclei. In the geometric view, they correspond to the three dynamical structures of the spherical vibrator, the axially symmetric deformed rotor, and the $\gamma$-unstable asymmetric deformed rotor [2]. In the proton and neutron (pn) IBM called IBM-2 the proton and neutron bosons are taken into account separately. The transitions between these limiting symmetries may be studied by their combinations for which numerical solutions have to be obtained. In the collective model, two other analytically solvable critical point symmetries, the E(5) on the U(5)-O(6) path [3] and the $X$(5) on the U(5)-SU(3) path [4] have been identified.

The critical point symmetries have enriched the study of the nuclear structure of the atomic nuclei. The light Ba and Xe isotopes ($N < 82$) were associated with the O(6) symmetry in early works [5,6]. Casten *et al.* [5] pointed out that the Xe isotopes ($N < 82$) are the best examples of O(6) nuclei. They introduced the cubic boson-boson interaction in the IBM-1 Hamiltonian [6] to generate the deviations from the O(6) symmetry towards the triaxial symmetry in heavier isotopes. The need to identify some of these isotopes with the E(5) and O(6) symmetries led to further experimental efforts to obtain new precise data on the eigenvalues and absolute E2 transition rates [7,8].

Even at the midshell $N = 66$, the $^{120}$Xe isotope is not well deformed. The energy ratio $R_{4/2} = E(4_1^+)/E(2_1^+)$ is $\sim 2.5$ [9,10] and the quadrupole deformation $\beta = 0.25$, which decreases further for higher $N$. The Xe isotopes are $\gamma$ soft [5,6] but at larger $N$ have features of the E(5) [7,8] symmetry. Coquard *et al.* [8] extended the decay scheme of $^{126}$Xe and from the Coulomb excitation experiment determined the precise absolute $B$(E2) values for transitions, which are important to define the symmetries in the spectrum of $^{126}$Xe. Here we review briefly the earlier works on the spectrum of $^{126}$Xe to establish the background.

In the early applications of the IBM-2**,** Novoselsky and Talmi [11] used the IBM-2 with boson energy parameter $\varepsilon$ taken from the E($2_1^+$) in $N = 82$ $^{136}$Xe in order to link with the shell model. They used larger quadrupole interaction and varied $\chi_\pi$, $\chi_\nu$, and the $\lambda$ term in the IBM-2 Hamiltonian to reproduce the spectra of $^{126,128}$Xe. Sevrin *et al.* [12] studied the variation of the nuclear structure with neutron number $N$ in $^{120-130}$Xe. They determined the effect of the various parameters of the IBM-2 Hamiltonian affecting the even-odd spin (OES) staggering in the $K^\pi = 2^+$ $\gamma$ bands and on the spacing in the $\tau$ multiplets in the O(6) pattern spectrum. The variation of the $\chi_n$ and $\chi_p$ coefficients in the qudrupole operator allowed the modification of the O(6) symmetry structure. Lieberz *et al.* [13] established the states of $K^\pi = 0_2^+$ and $K^\pi = 4^+$ bands in $^{126}$Xe with strong decay from the $K^\pi = 4^+$ band to $3_1^+$ and $4_2^+ = 4_\gamma$ states in the $K^\pi = 2^+$ $\gamma$ band. They noted the strong $\Delta\tau = \pm 1 E2$ transitions and the weak $\Delta\tau = 0, \pm 2$ transitions, and compared the experimental $B$(E2) ratios with the predictions of the IBM [1] and the asymmetric rotor-vibration

---

*Corresponding author: j.h.hamilton @vanderbilt.edu

model [14]. They ruled out the rigid asymmetric rotor model as a description of this nucleus.

von Brentano *et al.* [15] used the ratios of absolute B(E2) values in the ($I \rightarrow I-2$) transitions in the ground- state (g.s.) band ($I^\pi = 2_1^+, 4_1^+$, and $6_1^+$) of $A \approx 130$ nuclei to study the U(5)-O(6) transition. The ratios are slightly less for the O(6) symmetry than for U(5). But the small difference requires very precise B(E2) values from Coulomb excitation or lifetime data with less than 10% error margins. Mantica, Jr., *et al.* [16] studied the levels of $^{126}$Xe and deduced the relative E2 transition rates in $^{124-130}$Xe. The low-spin structure of $^{126}$Xe was investigated following the decay of 1.6-min $1^+$ $^{126}$Cs. Using $\gamma$-ray singles, $\gamma\gamma$ coincidences, and conversion-electron spectra, they extended the spectrum, and performed the IBM-2 calculation.

In the reaction work, using an OSIRIS-12 spectrometer, Seiffert *et al.* [17] extended the ground band up to $I^\pi = 20^+$, and the other positive- and negative-parity bands in $^{126}$Xe, and compared the data with the IBM model. Gade *et al.* [18] studied the low-spin states of the nucleus $^{126}$Xe by means of $\gamma$ spectroscopy using the fusion evaporation reaction $^{123}$Te($\alpha, n$) $^{126}$Xe, performed at the Cologne FN tandem accelerator. The $\gamma\gamma$ coincidence and singles spectra were measured with the OSIRIS-cube spectrometer. Besides the ground and the quasi-$\gamma$ bands many other low-lying states were observed. The $\gamma\gamma$ directional correlations from the oriented states were analyzed to determine the multipolarities of the $\gamma$ transitions. They observed dominant E2 transitions in this extended work.

Meyer *et al.* [19] applied the triaxial rotation vibration model (TRVM) to Ba and Xe isotopes with $A \approx 120$–130 and found that TRVM can reproduce the data as well as the IBM with regard to level energies and interband transition ratios. Leviatan *et al.* [20] pointed out that the O(5) is the common subgroup of the U(5) and O(6) symmetries so that the nuclei on the U(5) to O(6) transition path will exhibit O(5) characteristics in the ($\sigma = $ N, $\nu_\Delta = 0$) irrep, and one may have to distinguish them from exclusive O(6) characteristics from the decay of ($\sigma = $ N$-2$) irrep. Pan *et al.* [21] applied the fermion dynamic symmetry model (FDSM) to study $^{124-130}$Xe nuclei and compared with IBM results. Vogel *et al.* [22] deduced the effective $\gamma$-deformation variable from the calculated matrix elements of ($Q \times Q$) and ($Q \times Q \times Q)_{000}$ interactions using the simplified IBM Hamiltonian $H_{\text{IBM}}$ with only boson energy $\varepsilon$ and the *LL* terms. They used the consistent Q formalism.

In the microscopic approach, Fossion *et al.* [23] used the relativistic mean field (RMF) with the NL3 force to map the potential-energy surface (PES) for Pd-Gd isotopes for identifying the E(5), X(5), and prolate-oblate (PO) transition. They obtained flat PES for $^{126-130}$Xe isotopes.

It would be useful to study the complex muliband spectrum of $^{126}$Xe in a microscopic approach based on the shell model. The dynamic pairing plus quadrupole (DPPQ) model of Kumar-Baranger [24], and Kumar [25] provides an alternative approach to study the collective nuclear structure of medium mass nuclei. Kumar and Gupta [26] and Gupta and Kumar [27] applied the DPPQ model to the light Ba and Ce ($N < 82$) isotopes by adopting a suitable basis of single-particle Nilsson orbits. The capability of the DPPQ

model for studying the spectrum of $^{124}$Xe *vis a vis* the IBM symmetries is illustrated recently by Gupta in Ref. [28]. Here we study the change in the nuclear structure in $^{126}$Xe with the addition of two valence neutrons and establish its status on the U(5)-O(6) path. We also apply the algebraic IBM-1 for further support, which plays a complementary role to the microscopic treatment.

Here we note that, even if the level energies in the spectrum of $^{126}$Xe, follow the O(6) dynamic symmetry, the interband B(E2) values do not follow the strict $\Delta\tau$ and $\Delta\sigma$ equal to 1 and 0 selection rules. Therefore, we used the IBM-1 Hamiltonian (sets 1 and 2) which break both the O(6) and the O(5) symmetries as they have a $\chi$ parameter not equal to zero.

In Sec. II, we briefly review the salient features of the dynamic pairing plus the quadrupole DPPQ model [24–26] and of the interacting boson model [1]. In Sec. III we describe the special features of the Xe isotopes and the extensive results from the theory for $^{126}$Xe. Besides the static characteristics of the nucleus, and the energy-level spectrum, we also illustrate the interband transitions for the five rotation-vibration bands. The odd-even staggering of the levels in the $K^\pi = 2^+$ $\gamma$ band is displayed to determine its $\gamma$-soft character. The PES is illustrated. The discussion and the summary are given in Sec. IV.

## II. THEORY

### A. Dynamic pairing plus quadrupole model

Long ago, the Copenhagen School held the view that a nucleus finds its shape through the competition between the quadrupole force attempting to deform it and the pairing force trying to keep it spherical. Using this concept, Kumar and Baranger developed the dynamic version of the DPPQ model [24]. In Ref. [25] Kumar explained its later version, capable to derive the collective spectra up to spin $6^+$. The DPPQ Hamiltonian $H_{\text{DPPQ}}$ is built on spherical single-particle basis to which the quadrupole and pairing interactions are added on equal footing in the generalized Bogoliubov transformation method.

$$H_{\text{DPPQ}} = H_S + H_Q + H_P, \tag{1}$$

where,

$$H_S = \Sigma_\alpha \varepsilon_\alpha c_\alpha^+ c_\alpha, \qquad \alpha = nljm, \tag{2}$$

and

$$H_Q = (-)\tfrac{1}{2}\chi \, \Sigma_{\alpha\beta\gamma\delta} \Sigma_M \langle\alpha|Q_M|\gamma\rangle \langle\delta|Q_M|\beta\rangle C_\alpha^+ C_\beta^+ C_\delta C_\gamma. \tag{3}$$

The operator $Q_M = r^2 Y_{2M}(\theta, \varphi)$.

The quadrupole force is just the product of their quadrupole moments $\times(-\chi)$.

The pairing interaction is included in the form

$$H_P = (-)\tfrac{1}{4}g\Sigma s_\alpha s_\gamma C_\alpha^+ C_{\bar\alpha}^+ C_{\bar\gamma} C_\gamma, \qquad s = (-1)^{j-m}. \tag{4}$$

The Hartree-Fock-Bogoliubov technique implies self-consistency and treats the Q and P forces at equal footing.

The solution of the $H_{\text{DPPQ}}$ yields quasiparticle (q.p.) energies and q.p. wave functions. This is performed for a mesh of 92 points in the $(\beta, \gamma)$ space ($\beta = 0$–0.5; $\gamma = 0°$–60°). Using the standard relations, the parameters of the collective Bohr Hamiltonian $H_{\text{coll}}$ are derived for all the mesh points of the $(\beta, \gamma)$ space. Then a summation of the collective wave functions over the full $(\beta, \gamma)$ space provides the dynamics of the motion of the nuclear core. Thus, a full band mixing is achieved [25]. For the light mass region, the inert core is reduced to $N = Z = 40$. See Refs. [26,27] for Ba and Ce and Ref. [28] for $^{124}$Xe and references cited therein.

The DPPQ) model of Kumar-Baranger [24], and Kumar [25] even if old, is well suited to study the nuclear structure of the shape transitional nuclei for the predictions of the absolute $B$(E2) values and to predict the detailed nuclear structure of the shape transitional nuclei. The model is microscopic in the sense that the parameters of $H_{\text{coll}}$ are obtained from the solutions of $H_{\text{DPPQ}}$. The shape of the nucleus in $(\beta, \gamma)$ space is predicted from the model. The recent microscopic treatments differ in the use of alternative single-particle interactions but use the five-dimensional collective model Hamiltonian for the detailed study of the spectra. Li [29,30] used the same basic procedure as originally developed in the DPPQ model [24,25].

Slight variation of the quadrupole force strength $\chi = X_Q A^{-1.4}$(MeV) is allowed to approximately reproduce the energy scale in E($2_1^+$). Also the ($Z = 40$, $N = 40$) inert core effect is taken into account through the mass renormalization factor $F_B$, which multiplies all the inertial coefficients in $T_{\text{vib}}$ and $T_{\text{rot}}$ [Eq. (5)].

$$H_{\text{coll}} = V(\beta, \gamma) + T_{\text{vib}}(\beta, \gamma) + T_{\text{rot}}(\beta, \gamma), \quad (5)$$

$$H_{\text{coll}} \Psi_{\alpha \text{IM}} = E_I \Psi_{\alpha \text{IM}}, \quad (6)$$

$$\Psi_{\alpha \text{IM}} = \Sigma_{K = \text{even}, +\text{ve}} A_{\alpha IK}(\beta, \gamma) \phi^I_{MK}. \quad (7)$$

$\phi^I_{MK}$ are the symmetrized sums of the rotational $D$ functions, $A_{\alpha IK}(\beta, \gamma)$ are the intrinsic vibrational wave-function amplitudes [25]. Coefficient $\alpha$ is the counting index for the states of same spin $I$. This enables to predict the $K$ components of any state of a collective rotation-vibration band of the given nucleus.

### B. Interacting boson model-1

The IBM [1] is an elegant algebraic model, based on the $L = 0, 2$ $s$ and $d$ bosons, representing the correlated valence nucleon pairs (or hole pairs) [1]. In IBM-1, no distinction is made between the neutron and the proton bosons or hole and particle bosons. The conservation of boson numbers in the boson-boson interactions leads to the U(6) algebraic group, having three dynamic symmetry chains of U(5), SU(3), and O(6) subgroups. These symmetries correspond to the spherical vibrator, axially deformed rotor, and the $\gamma$-unstable triaxially deformed rotor. The transitions between the basic symmetries cover all the nuclei. The four-term MULT-form of the IBM Hamiltonian is given in Eq. (8) [1],

$$H_{\text{IBM}} = \varepsilon n_{\text{d}} + kQQ + k'LL + k''PP. \quad (8)$$

The $H_{\text{IBM}}$ is based on the shell model, but the parameters of $H_{\text{IBM}}$ are determined phenomenologically, based on the
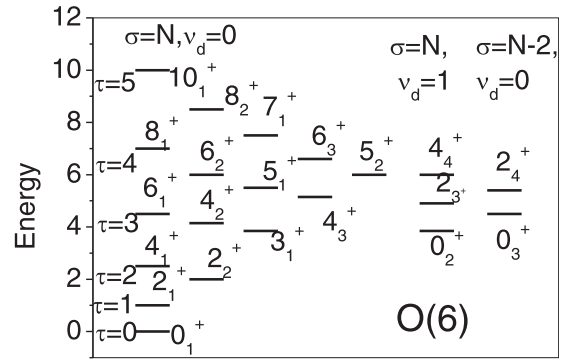


FIG. 1. Pattern of O(6) symmetry spectrum (partial), ($\nu_d = \nu_\Delta$).

energy-level data and on some specific $B$(E2) values as input. The computer program PHINT of Scholten [31] is used to set up the $H_{\text{IBM}}$.

### III. RESULTS OF CALCULATION IN THE IBM-1 AND DPPQ MODELS

#### A. The energy spectrum

The low-spin part of the O(6) spectrum (Fig. 1 adopted from Ref. [1]) is expressed in terms of the O(5) quantum number $\tau$ in the ($\sigma = $ N, $\nu_\Delta = 0$) multiplet (seen vertically), where $\sigma$ is the O(6) quantum number and $N$ is the total boson number ($N = N_p + N_n$). The O(6) symmetry spectrum is distinguished from a U(5) spectrum in having the second excited state of $I^\pi = 2_2^+$ below the $I^\pi = 4_1^+$ state in the $\tau = 2$ multiplet (seen horizontally). The quantum number $\nu_\Delta$ counts the boson triplets. The O(3) quantum number $L$ (for angular momentum) is used to split the $\tau$ multiplet. Also the $K^\pi = 0_2^+$ band belongs to the ($\sigma = $ N, $\nu_\Delta = 1$) multiplet, and the second excited state $0_3^+$ belongs to the ($\sigma = $ N$-2$, $\nu_\Delta = 0$) multiplet with its own characteristics. Real nuclei may lie on the U(5)-O(6) path. Both symmetries [U(5) and O(6)] have their own selection rules for transitions between the states. As a rule of thumb, the selection rules: $\Delta\sigma = 0$, $\Delta\tau = \pm 1$ are allowed and $\Delta\sigma > 0$ is a prohibited transition.

The O(6) spectrum is characterized by ($\tau = 1$, $I^\pi = 2_1^+$), ($\tau = 2$, $I = 4_1^+, 2_2^+$) states. Next, $\tau = 3$ irrep has ($I^\pi = 6_1^+$, $4_2^+, 3_1^+$), and the states based on the $0_2^+$ state with its own set of ($\tau = 0, 1, 2$) states in the ($\sigma = $ N, $\nu_\Delta = 1$) multiplet. The $\tau = 4$ irrep multiplet includes $8_1^+, 6_2^+, 5_1^+, 4^+$ ($K = 4$), $3_2^+$ (over $2_2^+$), and the $0_3^+$ state belonging to ($\sigma = $ N$-2$) irrep. In the U(5) limit, this $0_2^+$ state is also the part of the $\tau = 2$ irrep. Then $0_2^+$-$2_1^+$ is a $\Delta\tau = -1$ allowed transition. The $\tau = 5$ multiplet includes ($10_1^+, 8_2^+, 7_1^+, 6_3^+$, and $5_2^+$ states).

It is well recognized that the O(5) symmetry being the subgroup of both symmetries [U(5) and O(6)], many of these nuclei will exhibit the characteristics of O(5) [19,20]. Then it is an intricate task to identify the spectral features specific to O(6) symmetry and to study the deviations from O(6) selection rules.

In Fig. 2 the partial energy-level spectrum [9] of $^{118-130}$Xe isotopes is illustrated. There is slow and smooth variation of the low-lying states with neutron number $N$, but the movement
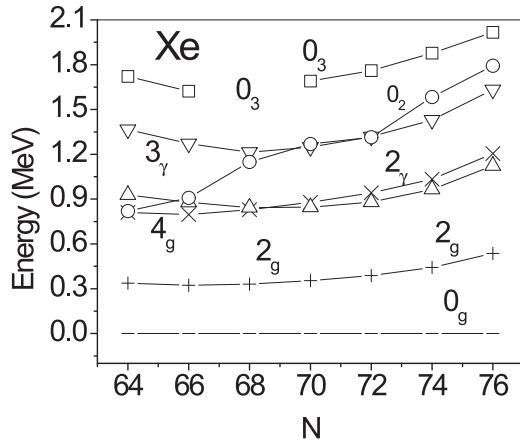
FIG. 2. The partial energy-level spectrum of $^{118-130}$Xe.



FIG. 4. Partial level energy spectrum of $^{126}$Xe in experiment.

of the $0_2^+$ state with $N$ is rather sharp and interesting. It signifies the underlying changing symmetry. In $N = 64$, 66 $^{118,120}$Xe, it is part of the $n = 2$ phonon triplet. But in $N = 72$ $^{126}$Xe it may be part of the $\tau = 3$ irrep, overlapping with the $3^+$ state. Compare it with Fig. 1 for O(6) symmetry. Overall (seen vertically), the $^{126}$Xe ($N = 72$) spectrum follows this O(6) pattern (Fig. 1) with the $2_2^+$ state below the $4_1^+$ and $0_2^+$ state up. Also see Figs. 3 and 4.

The energies in the O(6) dynamic chain are a linear combination of the quadratic Casimir operators of the O(6) group,

$$E(\sigma, \tau, I) = A(\sigma - N)(\sigma + N + 4)$$
$$+ B\tau(\tau + 3) + CI(I + 1). \quad (9)$$

For the $\sigma = N$ multiplet, the first term reduces to zero. For maximum spin $I$, the level spacing is given by the second term $B\tau(\tau + 3)$. This feature of the O(6) symmetry is equal to the O(5) symmetry. In Fig. 3 we illustrate the ground band energy-level (partial) spectrum of $^{126}$Xe, in comparison with the prediction of the O(5) symmetry common to U(5) and O(6) for spin up to $I^\pi = 12^+$. The $R_{I/2}$ values in $^{126}$Xe follow the O(5) curve with a small difference. At spin $I = 4$, the energy ratio $R_{4/2} = E(4_1^+)/E(2_1^+)$ is 2.24, slightly less than
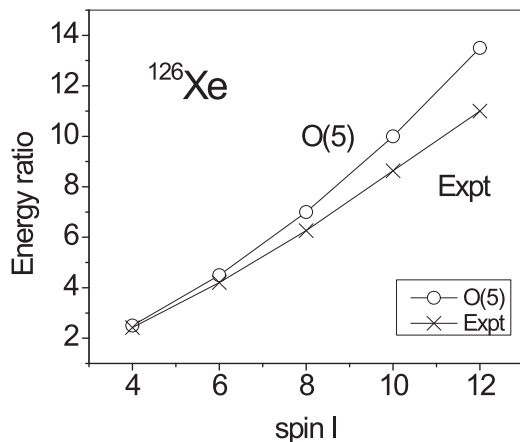
the O(5) value of 2.50. With increasing spin $I$, the deviation from the O(5) value increases. The small deviation at spin $I = 12$ from the O(5) curve signifies the rotation-vibration interaction effect or centrifugal stretching effect, increasing with spin $I$.

The partial energy-level spectrum [9] of $^{126}$Xe is illustrated in Fig. 4. Over all, it represents the pattern of the O(6) symmetry as stated above. The states in the first four columns belong to $\sigma = N$ irrep. The states over $0_2^+$ belong to the $\nu_\Delta = 1$ multiplet and the $0_3^+$ state belongs to the $\sigma = N-2$ multiplet.

In Table I, the level energies from the empirical fit in IBM-1 are compared with experiment and the DPPQ model for the ground-state band and the $K^\pi = 2^+$ $\gamma$-vibrational band. Table II lists the $K^\pi = 0_2^+$, $0_3^+$ bands and the $K^\pi = 4^+$ band. The values from the two sets of IBM-1 [Eq. (8)] with $H_{IBM}$ parameters listed in the caption of Table I are given. Set 2 yields slightly better overall agreement with the data. The energy values from the DPPQ model, slightly better than the IBM values (Table I), compare well with experiment. Although, both models yield somewhat high values for higher excited bands (Table II). The $4_3^+$ state is predominantly $K^\pi = 4^+$ in the DPPQ model. In IBM too, the $4_3^+$ state is included in the $K^\pi = 4^+$ band as also displayed in Fig. 5, which is supported by its E2 decay data with preference to decay to the $K^\pi = 2_\gamma$ $\gamma$ band (see below, Tables IV and VI). Here we



FIG. 3. Energy ratio $R_{I/2}$ of the ground band of $^{126}$Xe compared to O(5) symmetry.

TABLE I. Level energies (keV) of the ground and $K^\pi = 2^+$ $\gamma$ band in $^{126}$Xe. IBM-1 set 1 EPS = 666.6, $QQ = -50.4$, ELL = 11.9, PAIR = 30.5 keV, $\chi = 0.428$, set 2: EPS = 567.0, $QQ = 2k = -53.4$, ELL = 11.0, PAIR = 35.2 keV, $\chi = -0.428$ DPPQ model parameters $X = 71$, $F_B = 2.8$. $e_n = 0.65$, and $K$ components of each state predicted.

| Item | $2_1^+$ | $4_1^+$ | $6_1^+$ | $2_2^+$ | $3_1^+$ | $4_2^+$ | $5_1^+$ | $6_2^+$ |
|---|---|---|---|---|---|---|---|---|
| EXP [9] | 388.6 | 942 | 1635 | 879.9 | 1317.7 | 1488.4 | 1903 | 2214 |
| IBM set 1 | 424 | 1040 | 1828 | 1022 | 1704 | 1768 | 2576 | 2665 |
| Set 2 | 344 | 874 | 1576 | 888 | 1479 | 1548 | 2262 | 2353 |
| | | | | | | | | |
| DPPQ | 406 | 904 | 1500 | 974 | 1508 | 1569 | 2142 | 2245 |
| $K = 0$, % | 90.5 | 87.4 | 83.3 | 16.7 | 0.0 | 24.4 | 0.0 | 31.7 |
| $K = 2$, % | 9.5 | 10.8 | 14.3 | 83.3 | 100 | 51.1 | 87.8 | 40.7 |
| $K = 4$, % | | 1.8 | 1.80 | | | 24.5 | 12.3 | 19.5 |

TABLE II. Level energies (keV), $K$ components, $\beta_{\mathrm{rms}}$, and $\gamma_{\mathrm{rms}}$ values for higher excited bands in $^{126}$Xe.

| Spin | $0_2^+$ | $2_3^+$ | $4_4^+$ | $0_3^+$ | $2_4^+$ | $4_3^+$ | $5_2^+$ |
|---|---|---|---|---|---|---|---|
| EXP [9] | 1314 | 1679 | 2042 | 1760.5 | 2086[a] | 1903.1 | 2363.1 |
| IBM set 1 | 1370 | 2103 | 2975 | 1779 | 2527 | 2539 | 3471 |
| Set 2 | 1278 | 1947 | 2746 | 1682 | 2292 | 2236 | 3082 |
| | | | | | | | |
| DPPQ | 1266 | 1928 | 2612 | 1807 | 2453 | 2210 | 2874 |
| $K = 0$, % | 100 | 75.1 | 66.3 | 100 | 86.1 | 0.8 | 0.0 |
| $K = 2$, % | | 24.7 | 20.2 | | 13.9 | 40.0 | 15.9 |
| $K = 4$, % | | | 13.5 | | | 59.2 | 84.1 |
| $\beta_{\mathrm{rms}}$ | 0.205[b] | | | 0.202[b] | | | |
| $\gamma_{\mathrm{rms}}$ | 17.2 ° | | | 38.9 ° | | | |

[a]The $I^\pi = 2^+$ state at 2064 keV with large $M1$ to $2_1^+$ is considered as the mixed $F$-symmetric state [15].

[b]For the $0_1^+$ ground state the $\beta_{\mathrm{rms}}$, $\gamma_{\mathrm{rms}}$ values are 0.178, 27.3 °, and for the $2_1^+$ state are 0.194 and 25 °.

note that the $I_\gamma$ for E2 transitions from the $4_3^+$ state in Ref. [9] are not listed except $= 100$ for transition to the $2_2^+$ state, but the transitions to $4_1^+$, $3_1^+$, and $4_2^+$ are indicated. However, in Ref. [13], the relative $I_\gamma'$ s are given, which we have included in Table VI for comparison with theory.

The partial energy spectrum of $^{126}$Xe from the IBM-1 fit is illustrated in Fig. 5. The pattern of levels in the ground band and $K^\pi = 2^+$ $\gamma$ band, $K^\pi = 0_2^+$, $K^\pi = 4_1^+$, and $K^\pi = 0_3^+$ agrees with the O(6) pattern in Fig. 1 and the experimental spectrum in Fig. 4. The spin $2_2^+$ level overlaps with the spin $4_1^+$ level. The $K^\pi = 4_1^+$ band head lies at the $\tau = 4$ level (along with $6_2^+$ and $5_1^+$ levels. The $0_2^+$ state lies at $\tau = 3$ level along with the $3_1^+$ state, and the $0_3^+$ state lies at the $\tau = 4$ level.

The partial energy-level spectrum from the DPPQ model is illustrated in Fig. 6. Again, the pattern of levels agrees with O(6) in Fig. 1 and the experimental spectrum in Fig. 4. This is rather interesting. In the DPPQM calculation, the input data are the $Z$ and $N$ values of the given isotope, and as stated above, only two parameters are adjusted slightly (within a few percent), the rest of the parameters are the same for a broad region. No input data on level energies or $B$(E2) are input *ab initio*. That validates the composition of our DPPQ model (set up for midmass nuclei), adopted in Ref. [26] for ($N < 82$)
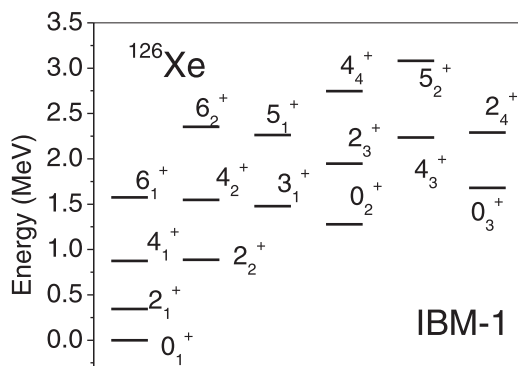


FIG. 5. Partial energy spectrum of $^{126}$Xe in IBM-1 (set 2).
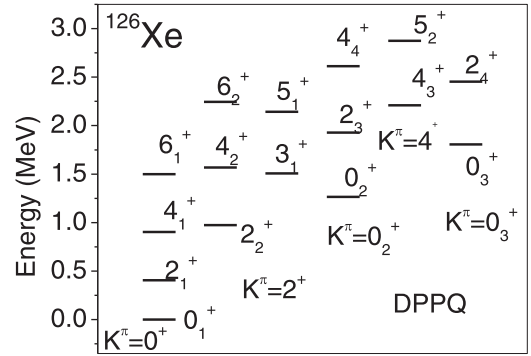


FIG. 6. Partial energy spectrum of $^{126}$Xe in the DPPQ model.

Ba isotopes with valence nucleons above $Z = 40$, the $N = 40$ inert core, and for $^{124}$Xe [28].

In the microscopic DPPQ model, one predicts the separate $K$-component contributions to the normalizing integral of a collective state. Although the ground-state band is largely $K^\pi = 0^+$, the other excited bands have significant $K$ admixtures. The $K^\pi = 2^+$ band has (17–32%) $K = 0$ admixture (increasing with spin $I$) (Table I), and the same is true for the $K^\pi = 0_2^+$ band (Table II). The $K^\pi = 0_3^+$, $I = 2_4$ level is relatively pure $K^\pi = 0^+$ to qualify as a quasi-$\beta$ band as termed in Ref. [8]. The less mixing for $\sigma = N-2$ for this state is also reflected. The $K^\pi = 4^+$ band has substantial $K = 2$ mixing Table II). This may also reflect in the stronger E2 transitions to the $K^\pi = 2^+$ $\gamma$ band (see Table IV). The finite admixtures are an indication of the nonaxial symmetry and the shift to O(6) symmetry.

### B. Absolute $B$(E2) values in $^{126}$Xe

In the recent Coulomb excitation experiment [8], precise values of interstate E2 transitions have been measured. Coquard *et al.* [8] also made careful fits in the IBM-1. The DPPQ model calculation are performed with only a slight variation of quadrupole force strength parameter $X$, which is set here to $X = 71.0$ along with the core renormalization factor $F_B = 2.8$. Compare this with the regional values of 70.0 and 2.4, respectively. We have also used the computer program PHINT [31]. The IBM-1 parameters are listed in Table I. Our $B$(E2, $2_1^+ \rightarrow 0_1^+$) in the DPPQ model is approximately equal to the data (Table III). The charge parameter $e_n = 0.65$, a regional value, is retained. In IBM-1, our value is larger, but no adjustment of the charge parameter has been performed. This does not affect the main conclusions from the predicted spectrum values.

In the DPPQ model, the variation in absolute $B$(E2) values for the $K^\pi = 2^+$ ($I = 2, 3, 4$) band to ($I = 0, 2, 4$) states of the ground band are well given (Table III). Our $B$(E2) values in IBM-1 are also in agreement with experiment and are as good as the IBM values from Ref. [8] (see the columns). The E2 transitions (varying through several orders of magnitude) in $^{126}$Xe, display the O(5) pattern rules of allowed $\Delta t = \pm 1$ and weak $\Delta \tau = 2$ transitions. The same are reflected in theory.

TABLE III. Absolute $B$(E2) values ($e^2b^2$) in the decay of $^{126}$Xe. (1 WU = 0.003752) Level energy of the initial state are in keV, $X = 71$, $F_b = 2.8$, and $e_n = 0.65$ for the DPPQ model. Charge parameters: 0.12 and $-0.12$ for IBM.

| Level | Initial | Final | EXP WU | $e^2b^2$ [8] | IBM [8] | IBM [a] | DPPQ |
|---|---|---|---|---|---|---|---|
| $Q(2_1^+)\, eb$ | $2_1^+$ | $2_1^+$ | | $-0.79$ | | $-0.55$ | $-0.625$ |
| 388 keV | $2_1^+$ | $0_1^+$ | 41.0 13 | 0.153 5[b] | 0.153 | 0.199 | 0.154 |
| 942 keV | $4_1^+$ | $2_1^+$ | 71.0 67 | 0.266 24 | 0.22 | 0.284 | 0.258 |
| 879 keV | $2_2^+$ | $2_1^+$ | 43.2 26 | 0.162 10 | 0.18 | 0.185 | 0.183 |
| | | $0_1^+$ | 0.63 7 | 0.0024 2 | 0.0024 | 0.0026 | 0.0032 |
| 1317 keV | $3_1^+$ | $4_1^+$ | $\leqslant$22.1 13 | $\leqslant$0.083 5 | 0.060 | 0.068 | 0.066 |
| | | $2_2^+$ | 55.7 63 | 0.210 22 | 0.17 | 0.204 | 0.231 |
| | | $2_1^+$ | 0.090 23 | 0.00033 8 | 0.0034 | 0.0043 | 0.0061 |
| 1488 keV | $4_2^+$ | $4_1^+$ | 28.3 38 | 0.106 13 | 0.097 | 0.101 | 0.111 |
| | | $2_2^+$ | 36.1 42 | 0.135 15 | 0.125 | 0.147 | 0.158 |
| | | $2_1^+$ | 0.40 8 | 0.0015 30 | 0.0005 | 0.0 | 0.0013 |
| 1903.5 keV | $5_1^+$ | $3_1^+$ | | | | 0.15 | 0.20 |

[a]In IBM only set 2 values are listed.
[b]The 0.165 (14) in the compilation [32].

The absolute $B$(E2) values for transitions from $I = 2_3$ of the $K^\pi = 0_2^+$ band and $I = 2_4$ of the $0_3^+$ band in Table IV are given fairly well in the DPPQ model as well as in IBM-1. Here, ($\Delta\sigma > 0$) weak transitions of the O(6) symmetry are operative. The $B$(E2) values for the $\tau = 3$, $4_3^+$ state of the $K^\pi = 4^+$ band in the DPPQ model and IBM-1 are mutually consistent. The values for transitions to the $K^\pi = 2_1^+$ band are relatively stronger than for the transition to the ground band.

### C. Interband $B$(E2) ratios in $^{126}$Xe

The $\gamma$-$g$ $B$(E2) ratios for the transitions from the spin $I = (2$–$6)$ to levels in the ground band and intraband transitions (Table V) are compared with DPPQ model predictions and our IBM-1 values and from other works [11,21,22]. The decay pattern is well reproduced in theory.

TABLE IV. Absolute $B$(E2) ($e^2b^2$) values for E2 transitions from $K^\pi = 0^+, 4^+$ bands.

| keV | $I_i$ | $I_f$ | EXP WU | EXP $e^2b^2$ | IBM [8] | Set 2 | DPPQ |
|---|---|---|---|---|---|---|---|
| 1314 | $0_2^+$ | $2_2^+$ | 64 9 | 0.24 3 | 0.22 | 0.21 | 0.141 |
| | | $2_1^+$ | 5.9 9 | 0.022 3 | 0.021 | 0.050 | 0.117 |
| 1679 | $2_3^+$ | $3_1^+$ | 20.6 44 | 0.077 15 | 0.106 | 0.084 | 0.091 |
| | | $0_2^+$ | 38.3 91 | 0.144 36 | 0.087 | 0.110 | 0.141 |
| | | $4_1^+$ | 0.96 4 | 0.0036 2 | 0.0051 | 0.020 | 0.049 |
| | | $2_2^+$ | $\leqslant$1.86 41 | 0.0069 14 | 0.0006 | 0.0082 | 0.023 |
| | | $2_1^+$ | 0.10 2 | 0.0004 1 | $7 \times 10^6$ | 0.0003 | 0.0004 |
| | | $0_1^+$ | 0.063 14 | 0.0002 1 | 0.0001 | 0.0006 | 0.0006 |
| 1760 | $0_3^+$ | $2_2^+$ | 13.4 41 | 0.050 15 | 0.018 | 0.066 | 0.145 |
| | | $2_1^+$ | 10.9 25 | 0.040 10 | 0.042 | 0.009 | 0.015 |
| 2086 | $2_4^+$ | $4_1^+$ | 1.63 16 | 0.0061 6 | 0.018 | 0.0023 | 0.0076 |
| | | $2_2^+$ | 0.99 61 | 0.0037 24 | 0.011 | 0.0025 | 0.009 |
| | | $2_1^+$ | 0.04 1 | $15 \times 10^{-5}$ | $30 \times 10^{-5}$ | 0.0001 | $6 \times 10^{-5}$ |
| 1903 | $4_3^+$ | $2_2^+$ | | | | 0.0007 | 0.0045 |
| | | $3_1^+$ | | | | 0.13 | 0.18 |
| | | $4_2^+$ | | | | 0.12 | 0.15 |
| | | $4_1^+$ | | | | 0.0006 | 0.0006 |

The $B$(E2) ratios for transitions from spins $2_3^+$ and $4_4^+$ of the $0_2^+$ band (Table VI) are small, and the ratios exhibit wide spread variation. The E2 transition from $\tau = 2$ over the $0_3^+$ state of ($\sigma = $N$-2$, 0) multiplet to $\tau = 2$, spin $4_1^+$ and $2_2^+$ of the ($o = $N, 0) multiplet are equally strong and given well in the DPPQ model and IBM. From the $\tau = 4$, $K^\pi = 4^+$, $I = 4$ states, stronger decay to the $K^\pi = 2^+$ $\gamma$ band is supported by theory.

### D. Energy staggering in the $K^\pi = 2^=\gamma$ band

For the odd -even staggering in the $K^\pi = 2^+$ $\gamma$ band, Casten et al. [33] defined

$$R_I = 2(E_I - E_{I-1})/(E_I - E_{I-2}), \quad (10)$$

and

$$R(I)_{\text{rotor}} = I/(I - 1/2) \text{ and spin} - \text{dependent index}, \quad (11)$$

$$S(I) = R_I/R_I(\text{rotor}) - 1. \quad (12)$$

According to Eq. (12), the staggering index $S$(4) is zero for the axially symmetric rotor and $-1.0$ for the spherical harmonic vibrator [degenerate ($4^+$, $3^+$)]. For even spin ($I$), $S(I)$ for $\gamma$-soft rotor or O(6) are negative, and for the rigid triaxial rotor are positive.

In Fig. 7 we illustrate the values of index $S(I)$ for $N = 70$, 72 $^{124,126}$Xe. The $S(I)$ variation with spin ($I$) is similar for the two isotopes with a minor increase in $^{126}$Xe. The negative values for even spin and positive values for odd spin, indicate the $\gamma$-soft status of both isotopes. The decrease in $|S(\text{I})|$ with increasing spin, indicates a move towards the axial symmetry or E(5) symmetry.

### E. PES $V(\beta, \gamma = 0°)$

The potential energy function of the collective Hamiltonian of Eq. (13) is calculated microscopically at each of the 92 points of a ($\beta, \gamma$) mesh ($0 < \beta < \beta_{\text{max}}$, $0° < \gamma < 60°$), The

TABLE V. $B$(E2) ratios in $^{126}$Xe in the IBM-1 and DPPQ models.

| $B$(E2) ratio | NNDC | IBM-2 | FDSM | IBM | IBM-1 | IBM-1 | DPPQ |
|---|---|---|---|---|---|---|---|
| $I_i$ $I_f/I_{f'}$ | [9] | [11] | [21] | [22] | Set 1 | Set 2 | |
| $Q(2_1^+)$ eb | −0.79 2 | | | | | −0.45 | −0.55 | −0.62 |
| $2_2^+ − 0_1/2_1$ | 0.014 1 | 0.038 | 0.014 | 0.015 | 0.007 | 0.014 | 0.018 |
| $3_1^+ − 2_2/2_1$ | 45 2 | 19 | 54 | 45 | 79 | 47 | 37 |
| $4_1/2_2$ | 0.40 3 | 0.43 | 0.40 | 0.37 | 0.42 | 0.30 | 0.29 |
| $2_1/4_1$ | 0.055 3 | 0.12 | 0.046 | 0.059 | 0.030 | 0.069 | 0.095 |
| $4_2^+ − 4_1/2_2$ | 0.86 4 | 0.95 | 0.91 | 0.80 | 0.75 | 0.69 | 0.70 |
| $2_1/2_2$ | 0.011 1 | 0.010 | 0.018 | 0.0002 | 0 | 0 | 0.008 |
| $2_1/4_1$ | 0.013 1 | 0.010 | 0.020 | 0.0003 | 0 | 0 | 0.012 |
| $5_1^+ − 4_1/3_1$ | 0.038 2 | 0.040 | | 0.008 | 0.0055 | 0.0088 | 0.023 |
| $4_2/3_1$ | 0.94 5 | 0.65 | | 0.45 | 0.46 | 0.465 | 0.50 |
| $4_1/6_1$ | 0.055 | 0.059 | | 0.019 | 0.02 | 0.025 | 0.069 |
| $6_2^+ − 4_1/4_2$ | 0.006 1 | | | | 0.0004 | 0.0003 | 0.002 |
| $6_1/4_2$ | 0.28 4 | | | | 0.31 | 0.39 | 0.34 |
| $0_2^+ − 2_1/2_2$ | 0.093 2 | 0.012 | 0.018 | 0.011 | 0.54 | 0.23 | 0.82 |

potential-energy function $V(\beta, \gamma)$ is given by three terms, viz. deformed state energy, pairing energy term, and quadrupole energy term [25],

$$V(\beta, \gamma) = \Sigma_{it} v_i^2 \eta_i - \Sigma_\tau g_\tau^{-1} \Delta_\tau^2 + \tfrac{1}{2} \chi^{-1} \beta^2. \quad (13)$$

Here "i" represents all deformed quasiparticle (dqp) states of the two oscillator shells, $v_i^2$ is the occupation probability of a dqp state, $\eta_i$ is the dqp energy, $g_\tau$ is the pairing strength ($\tau = n, p$), and $\Delta_\tau$ is the calculated pairing gap. The quadrupole strength $\chi = XA^{-1.4}$.

The plot of potential-energy surface $V(\beta, \gamma = 0°)$ for $^{126}$Xe, obtained from the DPPQ model solution, is given in Fig. 8. The minimum on the prolate side is −0.92 MeV at $\beta = 0.174$, and the prolate-oblate difference $V_{PO}$ is 0.5 MeV. However, the zero point energy level lies about 0.4 MeV above the $V = 0$ at $\beta = 0$. It results in the effective PES of a flat
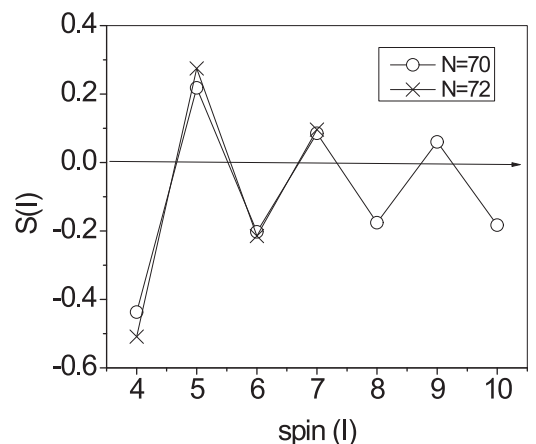
surface. Compared to the $V(\beta)$ for $^{124}$Xe [28], the depth of the PES is reduced, and the zero point level is raised. This is expected since the addition of two neutrons leads to smaller $\beta$ and larger $\gamma$. In view of Nilsson single-particle orbitals, the added neutrons occupy the rising orbitals. Our plot differs from the one obtained by Fossion *et al.* [23] using the RMF theory wherein they obtained a broad flat minimum. They have not plotted the zero point energy level. For an O(6)-like nucleus, a finite $V_{PO}$ is expected as obtained here from the DPPQ model calculation.

### F. Shape phase transition

In Table II, we have listed the values of $\beta_{rms}$ and $\gamma_{rms}$ as obtained in the DPPQ model calculation for the $0_1^+$ g.s., $2_1^+$ state, and $0_2^+, 0_3^+$ states. The PES minimum lies at 0.174 (Fig. 8), and $\gamma = 0°$. $\beta_{rms}$ and $\gamma_{rms}$ represent the dynamic values on the symmetry triangle, depending on the state wave function.

A slight increase in the quadrupole deformation parameter $\beta$ is expected for the rising energy of the state. Thus, the $\beta_{rms}$

TABLE VI. $B$(E2) ratios in $^{126}$Xe in the IBM-1 and DPPQ models, $K^\pi = 0_2^+, 0_3^+$, and $K^\pi = 4^+$ bands.

| $B$(E2) ratio | NNDC | IBM | IBM | DPPQ |
|---|---|---|---|---|
| $I_i$ $I_f/I_{f'}$ | [9] | Set 1 | Set 2 | |
| $2_3^+ − 0_2/2_2$ | 20 1 | 7.6 | 13.4 | 6.3 |
| $3_1/2_2$ | 11 1 | 3.5 | 10 | 4.1 |
| $2_1/4_1$ | 0.10 1 | 0.007 | 0.03 | 0.007 |
| $0_1/2_1$ | 0.61 3 | 2.5 | 2 | 1.8 |
| $0_1/0_2$ | 0.0017 1 | 0.005 | 0.5 | 0.004 |
| $2_1/0_2$ | 0.0027 2 | 0.002 | 0.003 | 0.002 |
| $4_4^+ 2_1/2_3$ | 0.10 | 0.0014 | 0.002 | 0.002 |
| $2_4^+ 4_1/0_1$ | 42 4 | | 23 | 76 |
| $2_2/4_1$ | 1.35 14 | 1.7 | 1.0 | 1.8 |
| $4_3^+ − 3/4_2$ | 0.43 13[a] | 1.17 | 1.15 | 1.2 |
| $2_2/4_2$ | 0.028 9[a] | 0.004 | 0.006 | 0.027 |
| $4_1/4_2$ | 0.045 14[a] | 0.004 | 0.005 | 0.004 |
| $5_2^+ − 4_2/3$ | 0.28 1[b] | 2.0 | 2.5 | 1.4 |
| $5_1/3$ | 34 2 | 354 | 250 | 35 |

[a]From Ref. [13].
[b]In Ref. [13] the value of 0.4 is listed.
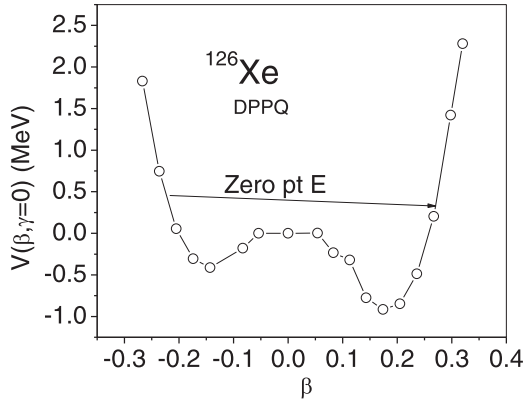


FIG. 7. Plot of OES index $S(I)$ for $^{124,126}$Xe.

FIG. 8. Plot of $V(\beta, \gamma = 0°)$ for $^{126}$Xe from the DPPQ model.

value is expected to increase with the rising level energy on account of the asymmetry in the potential. The values of $\beta_{\rm rms}$ for $0_1^+, 2_1^+, 0_2^+$, and $0_3^+$ reflect the same deformation. However, the $\gamma_{\rm rms}$ values for the four states are anomalous. The values of $27°$ and $25°$ for the ground band are normal, but the value of $17.2°$ for the $0_2^+$ state and $38.9°$ for $0_3^+$ are anomalous. These values represent the differing wave-function distributions on the $(\beta, \gamma)$ space.

In Ref. [28] for $^{124}$Xe, similar variations of $\beta_{\rm rms}$ and $\gamma_{\rm rms}$ were obtained. Therein the $A_{200}, A_{300}$ wave-function amplitude distribution on the $(\beta, \gamma)$ space were illustrated. The $\beta$ and $\gamma$ dependences of the $A_{200}$ and $A_{300}$ wave functions (see Figs. 10 and 11 in Ref. [28]) for the $0^+$ states are quite different both being different from the ground state. The calculated wave-function $A_{200}$ of the $0_2^+$ state has a node as a function of $\beta$ (at $\beta = 0.12$), shifted towards the spherical from $\beta_{\rm min}$, and for this reason looks as a wave function of the $\beta$-vibrational state. Correspondingly, the DPPQ model calculated $\Delta\tau = 2$ $B(E2, 0_2^+ \rightarrow 2_1^+)$ is finite ($=0.21$), slightly less than the $\Delta\tau = 1$, $B(E2, 0_2^+ \rightarrow 2_2^+)$ of $0.28e^2b^2$. The wave function of $0_3^+$, $A_{300}$ has its maximum on the oblate edge (Fig. 11 in Ref. [28]).

This is different from the plot of $A_{300}$ for the deformed nuclei where it exhibits a double node on the prolate edge. Similar features are expected for $^{126}$Xe.

## IV. SUMMARY AND DISCUSSION

In the present paper we have studied the $(N < 82)$ Xe isotopes with only four valence protons which are known to be $\gamma$ soft and to have the spectrum similar to the O(6) limiting symmetry. In contrast to the lighter $(N < 68)$ isotopes, the $N = 72$ $^{126}$Xe lies on the path of the increasing asymmetry parameter $\gamma$. Here we have analyzed the validity of the O(6) $\supset$ O(5) symmetry in the various vibrational bands of $^{126}$Xe. The ground band levels exhibit the O(5) symmetry, and the excited bands display the characteristics of the O(6) symmetry.

We have applied the microscopic theory of dynamic pairing plus quadrupole model and the algebraic interacting boson model-1. The energy spectrum, absolute $B(E2)$ values, the interband E2 transition rates, and their ratios are evaluated. The odd-even staggering in the $\gamma$ band is displayed, and the potential-energy plot is used to determine the shape of the nucleus.

The predictions of the eigenvalues and the $B(E2)$ values and the interband $B(E2)$ $B(E2)$ ratios, extended over the five excited bands up to $\tau = 5$ in the O(6) multiplet view are reproduced fairly well. The variations over four orders of magnitude are reproduced without any parameter adjustment. In IBM, we showed that the O(5) symmetry is well preserved, and the O(6) symmetry is slightly broken as in experiment. Thus, we have explored the $\gamma$ soft or O(6) status of $^{126}$Xe.

[1] F. Iachello and A. Arima, *The Interacting Boson Model* (Cambridge University Press, Cambridge, UK, 1987).

[2] A. Bohr and B. R. Mottelson, *The Nuclear Structure* (W. A. Benjamin, New York, 1975), Vol. II.

[3] F. Iachello, Phys. Rev. Lett. **85**, 3580 (2000).

[4] F. Iachello, Phys. Rev. Lett. **87**, 052502 (2001).

[5] R. F. Casten and P. von Brentano, Phys. Lett. B **152**, 22 (1981).

[6] R. F. Casten, P. von Brentano, K. Heyde, P. van Isacker, and J. Jolie, Nucl. Phys. A **439**, 289 (1985).

[7] L. Coquard *et al.*, Phys. Rev. C **80**, 061304(R) (2009).

[8] L. Coquard *et al.*, Phys. Rev. C **83**, 044318 (2011).

[9] Brookhaven National Laboratory, Chart of nuclides of National nuclear Data Center, http:\\www.nndc.bnl.gov/ensdf/.

[10] J. Katakura and K. Kitao, Nucl. Data Sheets **97**, 765 (2002).

[11] A. Novoselsky and I. Talmi, Phys. Lett. B **172**, 1399 (1986).

[12] A. Sevrin, K. Heyde, and J. Jolie, Phys. Rev. C **36**, 2631 (1987).

[13] W. Lieberz, A. Dewald, W. Frank, A. Gelberg, W. Krips, D. Lieberz, R. Wirowski, and P. Von Brentano, Phys. Lett. B **240**, 38 (1990).

[14] A. S. Davydov and G. F. Filippov, Nucl. Phys. **8**, 237 (1958).

[15] P. von Brentano, A. Gelberg, S. Harissopulos, and R. F. Casten, Phys. Rev. C **38**, 2386 (1988).

[16] P. F. Mantica, Jr., B. E. Zimmerman, W. B. Walters, J. Rikovska, and N. J. Stone, Phys. Rev. C **45**, 1586 (1992).

[17] F. Seiffert, W. Lieberz, A. Dewald, S. Freund, A. Gelberg, A. Granderath, D. Lieberz, R. Wirowski, and P. von Brentano, Nucl. Phys. A **554**, 287 (1993).

[18] A. Gade, I. Wiedenhöver, J. Gableske, A. Gelberg, H. Meise, N. Pietralla, and P. von Brentano, Nucl. Phys. A **665**, 268 (2000).

[19] U. Meyer, A. Faessler, and S. B. Khadkikar, Nucl. Phys. A **624**, 391 (1997).

[20] A. Leviatan, A. Novoselsky, and I. Talmi, Phys. Lett. B **172**, 144 (1986).

[21] X.-W. Pan, J.-L. Ping, D. H. Feng, J.-Q. Chen, C.-L. Wu, and M. W. Guidry, Phys. Rev. C **53**, 715 (1996).

[22] O. Vogel, P. Van Isacker, A. Gelberg, P. von Brentano, and A. Dewald, Phys. Rev. C **53**, 1660 (1996).

[23] R. Fossion, D. Bonatsos, and G. A. Lalazissis, Phys. Rev. C **73**, 044310 (2006).

[24] K. Kumar and M. Baranger, Nucl. Phys. A **110**, 529 (1968).

[25] K. Kumar, *Electromagnetic Interactions* (Hamilton, NH, 1975), Chap. 3, p. 35.

[26] K. Kumar and J. B. Gupta, Nucl. Phys. A **694**, 199 (2001).

[27] J. B. Gupta and K. Kumar, Nucl. Phys. A **882**, 21 (2012).

[28] J. B. Gupta, Nucl. Phys. A **927**, 53 (2014).

[29] Z. P. Li, T. Niksic, D. Vretenar, J. Meng, G. A. Lalazissis, and P. Ring, Phys. Rev. C **79**, 054301 (2009).

[30] Z. P. Li, T. Niksic, D. Vretenar, and J. Meng, Phys. Rev. C **81**, 034316 (2010).

[31] O. Scholten, *The Program Package* PHINT KVI-63, Groningen.

[32] B. Pritychenko, M. Birch, B. Singh, and M. Horoi, At. Data Nucl. Data Tables **107**, 1 (2016).

[33] R. F. Casten, N. V. Zamfir, P. von Brentano, F. Seiffert, and W. Lieberz, Phys. Lett. B **265**, 913 (1991).